PHYSICAL REVIEW B **91**, 174511 (2015)

Anomalous proximity effect and theoretical design for its realization

Satoshi Ikegaya,[1] Yasuhiro Asano,[1,2,3] and Yukio Tanaka[3,4]
[1]*Department of Applied Physics, Hokkaido University, Sapporo 060-8628, Japan*
[2]*Center of Topological Science and Technology, Hokkaido University, Sapporo 060-8628, Japan*
[3]*Moscow Institute of Physics and Technology, 141700 Dolgoprudny, Russia*
[4]*Department of Applied Physics, Nagoya University, Nagoya 464-8603, Japan*
(Received 12 November 2014; revised manuscript received 1 May 2015; published 15 May 2015)

We discuss the stability of zero-energy states appearing in a dirty normal metal attached to a superconducting thin film with Dresselhaus [110] spin-orbit coupling under an in-plane Zeeman field. The Dresselhaus superconductor preserves an additional chiral symmetry and traps more than one zero-energy state at its edges. All the zero-energy states at an edge belong to the same chirality in large Zeeman fields due to the effective p-wave pairing symmetry. The pure chiral nature of the wave function enables the zero-energy states to penetrate the dirty normal metal while retaining their high degree of degeneracy. We prove the perfect Andreev reflection into the dirty normal metal at zero energy.

DOI: 10.1103/PhysRevB.91.174511 PACS number(s): 74.81.Fa, 74.25.F−, 74.45.+c, 74.78.−w

I. INTRODUCTION

The proximity effect has been an important issue in the physics of superconductivity. In a normal metal attached to a spin-singlet s-wave superconductor, penetrating Cooper pairs form the *gap* structure in the quasiparticle density of states (DOS) at the Fermi level (zero energy) and modify low-energy properties there. In spin-triplet p-wave superconductor junctions, however, the penetrating Cooper pairs form a *zero-energy peak* in the DOS [1–3]. This induces various anomalous electromagnetic properties in the normal metal [4–6]. This effect is called the anomalous proximity effect. For instance, a perfect Andreev reflection from a p_x-wave superconductor into a dirty normal metal causes anomalous low-energy transport in the x direction such as a zero-bias conductance quantization in normal-metal/superconductor (NS) junctions [4] and a fractional current-phase relationship in superconductor/normal-metal/superconductor (SNS) junctions [3].

Recently, these characteristic transport phenomena have been investigated in the context of Majorana physics [7,8] based on the topological classification of materials [9]. In fact, as a consequence of the topologically nontrivial property of the wave function [10], the spin-triplet p_x-wave superconductor hosts more than one Majorana fermion at its edges. The energy dispersion of the topological edge states is flat as a function of the wave vector in the transverse direction (say k_y), which represents the high degree of the degeneracy in the zero-energy states (ZESs). The anomalous proximity effect stems from the penetration of such ZESs into the dirty normal metal while retaining their high degree of degeneracy [1,3,5]. Theoretically, it has been unclear what symmetry protects the high degeneracy of ZESs and why the perfect Andreev reflection persists at zero energy. It has been difficult to fabricate spin-triplet superconducting junctions using existing materials. However, the rapid progress in the Majorana physics of artificial superconductors [11–21] and in spintronics for controlling the spin-orbit interaction [22,23] has diffused the situation.

A set of three potentials is needed to realize topologically nontrivial superconductors artificially, namely the spin-orbit coupling, the Zeeman field, and the pair potential. Among them, the spin-orbit interaction mainly affects the energy spectra of the edge states. In InSb or GaAs, for example, the Dresselhaus spin-orbit interactions [24] are large in films growing along the [110] crystal direction. Theoretical studies [25,26] have shown that such artificial superconductors host more than one ZES similar to those of the p_x-wave superconductor. We also confirm that a proximitized spin helix thin film [22,23] also traps the flat ZESs with appropriate tuning of the Zeeman field. The Dresselhaus superconductors preserve an additional chiral symmetry independently of the particle-hole symmetry [9]. Recent theoretical studies [27–29] have shown that the chiral symmetry is responsible for the stability of more than one Majorana fermion. On the basis of the above novel insight, we solve an outstanding problem regarding the anomalous proximity effect.

In this paper, we first demonstrate the anomalous proximity effect of the Dresselhaus superconductors in large magnetic fields. After discussing the unitary equivalence between the Hamiltonian of Dresselhaus and spin-triplet p_x-wave superconductors, we analyze the chiral property of ZESs both at the edge of the superconductor and at the normal metal attached to it. The results show that all the ZESs have the same chirality due to the effective p_x-wave pairing symmetry. The pure chiral nature of the wave function is responsible for the robustness of highly degenerate ZESs in the presence of potential disorder. We will prove the perfect Andreev reflection from a p_x-wave superconductor into a dirty normal metal at zero energy. This paper provides a microscopic understanding of the anomalous proximity effect and a design for an artificial p_x-wave superconductor.

II. CONDUCTANCE QUANTIZATION

First, we numerically demonstrate the anomalous proximity effect of the Dresselhaus superconductor. Let us consider an NS junction on a two-dimensional tight-binding model with the lattice constant a_0 as shown in Fig. 1. A lattice site is indicated by a vector $\boldsymbol{r} = j\boldsymbol{x} + m\boldsymbol{y}$, where $\boldsymbol{x}$ ($\boldsymbol{y}$) is the vector in the x (y) direction with $|\boldsymbol{x}| = |\boldsymbol{y}| = a_0$. The present junction consists of three segments: an ideal lead wire ($-\infty \leqslant j \leqslant 0$), a normal disordered segment ($1 \leqslant j \leqslant L/a_0$),

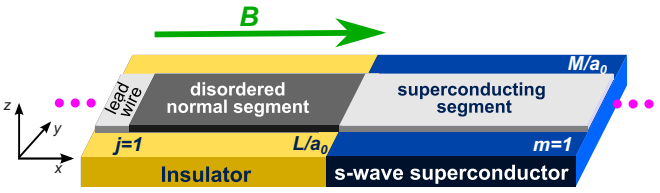

FIG. 1. (Color online) Schematic image of the NS junction of a Dresselhaus superconductor. The superconductor proximitizes the InSb thin film, which is grown along the [110] crystal direction.

and a superconducting segment ($L/a_0+1 \leqslant j \leqslant \infty$). The Hamiltonian reads

$$\begin{aligned}\hat{H}_0 =& -t\sum_{\sigma=\uparrow,\downarrow}\sum_{j}\sum_{m=1}^{M/a_0}\{c^\dagger_{\boldsymbol{r}+\boldsymbol{x},\sigma}c_{\boldsymbol{r},\sigma}+c^\dagger_{\boldsymbol{r},\sigma}c_{\boldsymbol{r}+\boldsymbol{x},\sigma}\}\\ &-t\sum_{\sigma=\uparrow,\downarrow}\sum_{j}\sum_{m=1}^{M/a_0-1}\{c^\dagger_{\boldsymbol{r}+\boldsymbol{y},\sigma}c_{\boldsymbol{r},\sigma}+c^\dagger_{\boldsymbol{r},\sigma}c_{\boldsymbol{r}+\boldsymbol{y},\sigma}\}\\ &+\sum_{\boldsymbol{r},\sigma}[4t-\mu]c^\dagger_{\boldsymbol{r},\sigma}c_{\boldsymbol{r},\sigma}+\sum_{j>L/a_0,m}\Delta_0(c^\dagger_{\boldsymbol{r},\uparrow}c^\dagger_{\boldsymbol{r},\downarrow}+\text{H.c.})\\ &-\sum_{\boldsymbol{r},\sigma,\sigma'}V_{ex}(\sigma_1)_{\sigma,\sigma'}c^\dagger_{\boldsymbol{r},\sigma}c_{\boldsymbol{r},\sigma'}+\sum_{1\leqslant j\leqslant L/a_0,m,\sigma}V_{\rm imp}(\boldsymbol{r})c^\dagger_{\boldsymbol{r},\sigma}c_{\boldsymbol{r},\sigma}\\ &-i\frac{\lambda_D}{2a_0}\sum_{\boldsymbol{r},\sigma,\sigma'}(\sigma_3)_{\sigma,\sigma'}(c^\dagger_{\boldsymbol{r}+\boldsymbol{x},\sigma}c_{\boldsymbol{r},\sigma'}-c^\dagger_{\boldsymbol{r},\sigma}c_{\boldsymbol{r}+\boldsymbol{x},\sigma'}),\end{aligned}\tag{1}$$

where $c^\dagger_{\boldsymbol{r},\sigma}$ ($c_{\boldsymbol{r},\sigma}$) is the creation (annihilation) operator of an electron at the site $\boldsymbol{r}$ with spin $\sigma=(\uparrow$ or $\downarrow)$, $t=\hbar^2/(2ma_0^2)$ denotes the hopping integral between the nearest-neighbor sites, m is the effective mass of an electron, μ is the chemical potential, and λ_D represents the strength of the Dresselhaus [110] spin-orbit interaction. By tuning the magnetic field B in the x direction, it is possible to introduce the external Zeeman potential V_{ex}. The parameters t, μ, λ_D, and V_{ex} are common to the superconductor and the normal metal. In the y direction, the number of lattice sites is M/a_0 and the hard-wall boundary condition is applied. The Pauli matrices in spin space are represented by $\hat{\sigma}_j$ for $j=1$–3 and the unit matrix in spin space is $\hat{\sigma}_0$. We consider the impurity potential given randomly in the $-W/2 \leqslant V_{\rm imp}(\boldsymbol{r}) \leqslant W/2$ range in the normal segment ($1 \leqslant j \leqslant L/a_0$) and the s-wave pair potential Δ_0 in the superconducting segment ($L/a_0+1 \leqslant j \leqslant \infty$).

We calculate the differential conductance $G_{\rm NS}$ of the NS junctions based on the formula [30]

$$G_{\rm NS}(eV)=\frac{e^2}{h}\sum_{\zeta,\eta}\left[\delta_{\zeta,\eta}-\left|r^{ee}_{\zeta,\eta}\right|^2+\left|r^{he}_{\zeta,\eta}\right|^2\right]_{eV=E},\tag{2}$$

where $r^{ee}_{\zeta,\eta}$ and $r^{he}_{\zeta,\eta}$ denote the normal and Andreev reflection coefficients at energy E, respectively. The indices ζ and η label the outgoing and incoming channels, respectively. These reflection coefficients are obtained by using the lattice Green's function method [31–33]. With this method, it is possible to calculate the transport coefficients exactly even in the presence of random impurity potentials. In Fig. 2, we show the differential conductance of the Dresselhaus superconductors as a function of the bias voltage for several lengths of disordered

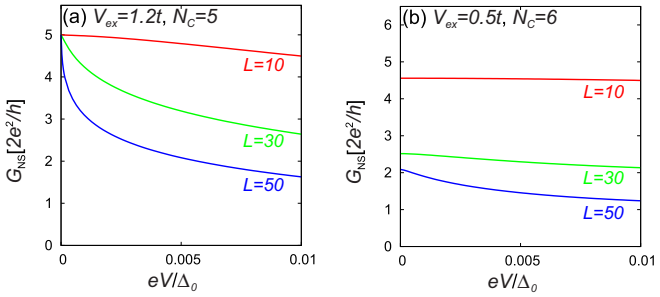

FIG. 2. (Color online) The differential conductance is plotted as a function of the bias voltage for several lengths of disordered segment L in units of a_0. In (a), the Zeeman potential $V_{ex}=1.2t$ is chosen that is larger than a critical value of $V_c=0.92t$. The number of propagating channels N_c is 5. In (b), we choose $V_{ex}=0.5t<V_c$ leading to $N_c=6$.

segments L, where we choose parameters of $\mu=1.0t$, $\lambda_D=0.2ta_0$, $W=2.0t$, $M=10a_0$, and $\Delta_0=0.1t$. The results are normalized to $G_Q=2e^2/h$. In Fig. 2(a), we choose $V_{ex}=1.2t$, which leads to the propagating channel number $N_c=5$. The differential conductance decreases with increasing L for finite bias voltages. However, the zero-bias conductance is quantized at G_QN_c irrespective of L. The results suggest that there are N_c perfect transmission channels in a disordered normal segment [4]. The conductance quantization at zero bias is an aspect of the anomalous proximity effect. We have also confirmed the fractional current-phase relationship in SNS junctions [3,34]. Such anomalous behaviors can be seen when the Zeeman field exceeds a critical value $V_{ex}>V_c=\sqrt{\mu_0^2+\Delta_0^2}$ with $\mu_0=\mu-2t\,[1-\cos\{\pi/(M/a_0+1)\}]$. With the present parameter choice, we obtain $V_c=0.92t$. On the other hand for $V_{ex}<V_c$, the conductance quantization is absent as shown in Fig. 2(b), where we choose $V_{ex}=0.5t<V_c$. The zero-bias conductance quantization at G_QN_c is a robust phenomenon in the topologically nontrivial phase described by $V_{ex}>V_c$ and $\lambda_D\neq 0$ and is independent of such parameters as M, W, and μ. In the experiment [18], for instance, the condition $V_{ex}>V_c$ may be satisfied under a magnetic field of less than 1 T in InSb nanowires owing to its large g factor and small Fermi energy. Inversion symmetry in the z direction is broken in the junction shown in Fig. 1. In such case, Rashba spin-orbit interaction $\lambda_R(k_y\hat{\sigma}_1-k_x\hat{\sigma}_2)$ is not negligible. Unfortunately, the Rashba term easily destroys the conductance quantization at zero bias because it breaks chiral symmetry discussed below. To delete the Rashba term, we need to recover inversion symmetry by attaching an appropriate insulator or the same superconductor on top of the InSb thin film.

III. MORE THAN ONE MAJORANA FERMION

Second, we analyze the chiral property of the ZESs. In what follows, we consider a Dresselhaus superconductor in continuous space for simplicity. The Hamiltonian is represented by

$$\check{H}_0=\begin{bmatrix}\hat{h} & i\Delta_0\hat{\sigma}_2\\ -i\Delta_0\hat{\sigma}_2 & -\hat{h}^*\end{bmatrix},\tag{3}$$

$$\hat{h}=\xi_{\boldsymbol{r}}\hat{\sigma}_0-V_{ex}\hat{\sigma}_1+i\lambda_D\partial_x\hat{\sigma}_3+V_{\rm imp}(\boldsymbol{r})\hat{\sigma}_0,\tag{4}$$

with $\xi_{\boldsymbol{r}} = \frac{-\hbar^2}{2m}\nabla^2 - \mu$. In the superconductor, we consider the uniform pair potential Δ_0 and ignore the impurity potential $V_{\rm imp} = 0$. In the normal metal, on the other hand, we introduce the impurity potential and do not consider the pair potential. We assume a sufficiently large Zeeman potential so that $\alpha_D \equiv \lambda_D k_F / V_{ex} \ll 1$ is satisfied with $k_F = \sqrt{2m\mu}/\hbar$.

By applying the unitary transformations as shown in Appendix B, H_0 is transformed into $\check{H}_1 = \check{H}_P + \check{V}_\Delta$ within the first order of α_D, where

$$\check{H}_P = \begin{bmatrix} \hat{H}_\uparrow & 0 \\ 0 & \hat{H}_\downarrow \end{bmatrix}, \ \check{V}_\Delta = \begin{bmatrix} 0 & i\Delta_0\hat{\sigma}_2 \\ -i\Delta_0\hat{\sigma}_2 & 0 \end{bmatrix}, \quad (5)$$

$$\hat{H}_\sigma = \begin{bmatrix} \xi_{\boldsymbol{r}} + s_s V_{ex} + V_{\rm imp} & -s_s \frac{\lambda_D \Delta_0}{V_{ex}} \partial_x \\ s_s \frac{\lambda_D \Delta_0}{V_{ex}} \partial_x & -\xi_{\boldsymbol{r}} - s_s V_{ex} - V_{\rm imp} \end{bmatrix}, \quad (6)$$

and $s_s = 1$ (-1) for $\sigma = \uparrow$ $(\downarrow)$. A Hamiltonian $\hat{H}_\sigma$ with $V_{\rm imp} = 0$ is equivalent to that of a spin-triplet p_x-wave superconductor and $\check{V}_\Delta$ mixes the two spin sectors. In the topologically nontrivial phase $V_{ex} > V_c$, all the spin-$\uparrow$ states pinch off from the Fermi level and only the spin-$\downarrow$ states remain at the Fermi level. Therefore the spin-mixing term $\check{V}_\Delta$ does not affect the remaining spin-$\downarrow$ states at all. In this way, we can shrink the 4×4 Hamiltonian $\check{H}_1$ of the Dresselhaus superconductor to the 2×2 Hamiltonian $\hat{H}_\downarrow$ of the p_x-wave superconductor. We assumed the two conditions $\lambda_D k_F \ll V_{ex}$ and $V_{ex} > V_c$ independently. To realize the p_x-wave superconductor, they can be unified into one condition $\lambda_D k_F \ll V_c$, which is accessible in the experiment [18]. The Hamiltonian $\hat{H}_\downarrow$ preserves a chiral symmetry

$$\hat{\tau}_1 \, \hat{H}_\downarrow \, \hat{\tau}_1 = -\hat{H}_\downarrow, \quad \hat{\tau}_1 = \begin{bmatrix} 0 & 1 \\ 1 & 0 \end{bmatrix}, \quad (7)$$

where $\hat{\tau}_j$ for $j = 1$–3 are the Pauli matrices in Nambu space. Here we summarize two important features of the eigenstates of $\hat{H}_\downarrow$ proved in Ref. [10]. (See also Appendix A for details.)

(i) The eigenstates of $\hat{H}_\downarrow$ at zero energy are simultaneously the eigenstates of $\hat{\tau}_1$. Namely, the eigenvectors at zero energy $\varphi_{\nu_0,\lambda}(\boldsymbol{r})$ satisfy

$$\hat{H}_\downarrow \, \varphi_{\nu_0,\lambda}(\boldsymbol{r}) = 0, \qquad \hat{\tau}_1 \, \varphi_{\nu_0,\lambda}(\boldsymbol{r}) = \lambda \, \varphi_{\nu_0,\lambda}(\boldsymbol{r}), \quad (8)$$

where $\lambda = \pm 1$ represents the eigenvalue of $\hat{\tau}_1$ and ν_0 is the index of the ZESs. We have omitted the spin index from the subscripts of $\varphi_{\nu_0,\lambda}$ because spin is always $\downarrow$.

(ii) In contrast to the zero-energy states, the nonzero-energy states are not the eigenstates of $\hat{\tau}_1$. They are described by the linear combination of two states: one has $\lambda = 1$ and the other has $\lambda = -1$. Below we prove the robustness of the highly degenerate ZESs in a dirty normal segment and the perfect Andreev reflection by taking these features into account.

In an isolating Dresselhaus superconductor (i.e., $-L \leqslant x \leqslant L$ and $0 \leqslant y \leqslant M$), we can describe the wave function of the zero-energy state for each transport channel. From the second equation in Eq. (8), it is given by

$$\varphi_{n,\lambda}(\boldsymbol{r}) = \chi_{n,\lambda}(x) \, Y_n(y) \begin{bmatrix} 1 \\ \lambda \end{bmatrix}, \quad (9)$$

where $Y_n(y) = \sqrt{2/M}\sin(n\pi y/M)$ is the wave function in the y direction with the hard-wall boundary condition and n indicates the transport channel. In the x direction, we also apply the hard-wall boundary condition at its edges, $\chi_{n,\lambda}(-L) = \chi_{n,\lambda}(L) = 0$. By substituting Eq. (9) into the first equation in Eq. (8), we obtain

$$\left[\partial_x^2 - 2\frac{\lambda}{\xi_D}\partial_x + k_n^2\right]\chi_{n,\lambda}(x) = 0, \quad (10)$$

where $\xi_D = \xi_0/\alpha_D$, $\xi_0 = \hbar v_F/\Delta_0$, $k_n = \sqrt{2m(\mu + V_{ex} - \epsilon_n)}/\hbar$, and $\epsilon_n = (\hbar n\pi/M)^2/(2m)$ is the kinetic energy in the y direction. The superconductor must be long enough to satisfy $L/\xi_D \gg 1$. We find the following two solutions for each propagating channel:

$$\varphi^L_{n,-}(\boldsymbol{r}) = \frac{C_L}{\sqrt{2}}\begin{bmatrix} 1 \\ -1 \end{bmatrix}\sin[q_n(x+L)]e^{-x/\xi_D}\, Y_n(y), \quad (11)$$

$$\varphi^R_{n,+}(\boldsymbol{r}) = \frac{C_R}{\sqrt{2}}\begin{bmatrix} 1 \\ 1 \end{bmatrix}\sin[q_n(x-L)]e^{x/\xi_D}\, Y_n(y), \quad (12)$$

with $q_n^2 = k_n^2 - \xi_D^{-2}$, where C_L and C_R are the normalization coefficients. We choose the gauge so that the wave functions in Eqs. (11) and (12) are real values. All the ZESs at the left (right) edge have $\lambda = -1$ $(\lambda = 1)$, which is shown schematically in Fig. 3.

In the Bogoliubov transformation, the field operator of an electron with spin-$\downarrow$ is generally described as

$$\begin{bmatrix} \Psi(\boldsymbol{r}) \\ \Psi^\dagger(\boldsymbol{r}) \end{bmatrix} = \sum_\nu [\varphi_\nu(\boldsymbol{r})\gamma_\nu + \hat{\Xi}\varphi_\nu(\boldsymbol{r})\gamma_\nu^\dagger], \quad (13)$$

$$\hat{\Xi} = \hat{\tau}_1 \mathcal{K}, \quad \hat{\Xi}\hat{H}_\downarrow\hat{\Xi}^{-1} = -\hat{H}_\downarrow, \quad (14)$$

where $\gamma_\nu^\dagger$ (γ_ν) is the creation (annihilation) operator of the Bogoliubov quasiparticle belonging to E_ν and $\hat{\Xi}$ is the charge conjugation operator with $\mathcal{K}$ indicating a complex conjugation. Equation (14) represents the particle-hole symmetry of the Hamiltonian. From Eq. (13), we can extract the electron field operator of the ZES at the nth propagating channel as

$$\Psi_n(\boldsymbol{r}) = i\gamma_n^L(\boldsymbol{r}) + \gamma_n^R(\boldsymbol{r}), \quad (15)$$

$$\gamma_n^L(\boldsymbol{r}) = -i\varphi^L_{n,-}(\boldsymbol{r})[\gamma_{n-} - \gamma_{n-}^\dagger], \quad (16)$$

$$\gamma_n^R(\boldsymbol{r}) = \varphi^R_{n,+}(\boldsymbol{r})[\gamma_{n+} + \gamma_{n+}^\dagger]. \quad (17)$$

The operator $\gamma_n^L(\boldsymbol{r})$ is purely imaginary while $\gamma_n^R(\boldsymbol{r})$ is real in the present gauge choice. They satisfy the Majorana relation $[\gamma_n^{L(R)}(\boldsymbol{r})]^\dagger = \gamma_n^{L(R)}(\boldsymbol{r})$. Therefore, the number of Majorana fermions at each edge is equal to the number of propagating

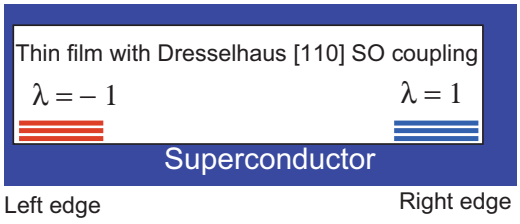

FIG. 3. (Color online) Schematic image of ZESs at two edges of an isolating Dresselhaus superconductor for $V_{ex} > V_c$. The number of the ZESs at either edge is equal to N_c. All of the ZESs at the left (right) edge have $\lambda = -1$ $(\lambda = 1)$.

channels at the spin-↓ sector $N_\downarrow$. Since there are no spin-↑ channels for $V_{ex} > V_c$, $N_\downarrow$ is equal to N_c. They are degenerate at zero energy at the same place. Such highly degenerate states may be fragile in the presence of a random impurity potential near the edges. However, at the left edge for example, all of the ZESs have $\lambda = -1$ as shown in Eq. (11). According to property (ii), such highly degenerate ZESs are robust against potential disorder because the random potentials preserve the chiral symmetry and the ZESs with $\lambda = 1$ are absent.

IV. PERFECT ANDREEV REFLECTION AND CHIRAL NATURE

Finally and most importantly, we prove the stability of the highly degenerate ZESs in a normal metal. To analyze the conductance of the NS junction, we attach a normal metal to the left side of the superconductor as shown in Fig. 1. The Hamiltonian of the normal metal is given by $H_\downarrow$ in Eq. (6) with $\Delta_0 = 0$. In the absence of impurity potentials, the wave function in the normal segment at $E = 0$ is described by

$$\varphi_N(\boldsymbol{r}) = \sum_n \left(\begin{bmatrix} 1 \\ r_n^{he} \end{bmatrix} e^{ik_n x} + \begin{bmatrix} r_n^{ee} \\ 0 \end{bmatrix} e^{-ik_n x} \right) Y_n(y), \tag{18}$$

where r_n^{ee} (r_n^{he}) is the normal (Andreev) reflection coefficient at channel n and $k_n = \sqrt{2m(\mu - \epsilon_n)}/\hbar$. The current conservation law implies $|r_n^{ee}|^2 + |r_n^{he}|^2 = 1$ at $E = 0$ for each channel. From the boundary conditions at the NS interface, the reflection coefficients are calculated to be

$$r_n^{ee} = 0, \quad r_n^{he} = -1, \tag{19}$$

for all n. The wave function in Eq. (18) is the eigenstate of $\hat{\tau}_1$ belonging to $\lambda = -1$ (i.e., $\varphi_N \propto [1, -1]^{\mathrm{T}}$), as well as the ZESs at the left edge of the superconductor. According to property (ii), they cannot form nonzero-energy states. Therefore, the ZESs can penetrate into the normal segment while retaining a high degree of degeneracy. The conclusion is also valid even in the presence of potential disorder because the impurity potential V_{imp} preserves the chiral symmetry and does not damage the pure chiral feature of the ZESs. This fact is unique to the p_x-wave pairing symmetry. In the ballistic limit, perfect conductance quantization at zero bias is a common property of unconventional superconductors that have the edge ZESs with a flat dispersion. For instance, in a spin-singlet d-wave superconductor with $\Delta_{\boldsymbol{k}} \propto k_x k_y$ [35], $|r_{k_y}^{he}| = 1$ holds for all transverse momentum values k_y. The Hamiltonian of d-wave superconductors also preserves the chiral symmetry. However, the highly degenerate ZESs are fragile under the potential disorder because the ZESs with two different chiralities coexist at the same edge [10]. Namely, the sign of $r_{k_y}^{he}$ depends on k_y. Therefore the presence of the chiral symmetry is not a sufficient condition for the anomalous proximity effect but a necessary one.

In a p_x-wave junction, all the ZESs in a normal metal have the same chirality of $\lambda = -1$ in the same way as the ZESs at the left edge of the superconductor. The pure chiral feature of the ZESs enables us to explain the perfect Andreev reflection into the dirty normal segment. According to property (i), the ZESs must be the eigenstate of $\hat{\tau}_1$. We emphasize that the wave function in Eq. (18) can be the eigenstate of $\hat{\tau}_1$ with $\lambda = -1$ only when Eq. (19) is satisfied. Although the channel index n is no longer a good quantum number under the potential disorder, all the wave functions in the normal segment have the same vector structure reflecting their pure chiral nature. This is a mathematical requirement arising from the chiral symmetry. The physical consequence of the vector structure is the perfect Andreev reflection into the dirty normal metal at $E = 0$. This explains the perfect quantization of the zero-bias conductance at $2e^2 N_c/h$.

V. CONCLUSION

In conclusion, we have discussed the stability of highly degenerate zero-energy states (ZESs) appearing in disordered junctions consisting of a superconducting thin film with Dresselhaus [110] spin-orbit coupling. The Dresselhaus superconductor hosts more than one ZES at its edges. When we make a normal-metal/superconductor junction of the Dresselhaus superconductor, such highly degenerate ZESs can penetrate into the dirty normal segment and form resonant transmission channels there. An analysis of the wave function in the normal segment shows that all the ZESs have the same chirality due to the effective p_x-wave pairing symmetry. The perfect Andreev reflection into the dirty normal metal is a direct consequence of the pure chiral feature of the ZESs. Our paper provides a microscopic understanding the anomalous proximity effect of the spin-triplet p_x-wave superconductor.

ACKNOWLEDGMENTS

The authors are grateful to J. D. Sau for useful discussions. This work was supported by "Topological Quantum Phenomena" (No. 22103002, No. 22103005) and KAKENHI (No. 26287069) from the Ministry of Education, Culture, Sports, Science, and Technology (MEXT) of Japan and by the Ministry of Education and Science of the Russian Federation (Grant No. 14Y.26.31.0007).

APPENDIX A: ZERO-ENERGY STATES UNDER A CHIRAL SYMMETRY

Here, we briefly summarize the argument in Ref. [10] which shows the important properties of zero-energy states under a chiral symmetry. We consider the BdG Hamiltonian H which preserves the chiral symmetry

$$\Gamma H \Gamma^{-1} = -H, \quad \Gamma^2 = 1. \tag{A1}$$

The relation is equivalent to

$$[H^2, \Gamma] = 0. \tag{A2}$$

The BdG equation is given by

$$H\varphi_E(\boldsymbol{r}) = E\varphi_E(\boldsymbol{r}). \tag{A3}$$

When we consider the eigenequation of H^2,

$$H^2 \chi_{E^2}(\boldsymbol{r}) = E^2 \chi_{E^2}(\boldsymbol{r}), \tag{A4}$$

Equation (A2) suggests that the eigenstate $\chi_{E^2}(\boldsymbol{r})$ is also the eigenstate of Γ at the same time. Since $\Gamma^2 = 1$, we find that the eigenvalue of Γ is $+1$ or -1. Namely the

eigenequation

$$\Gamma\chi_{E^2\lambda}(\boldsymbol{r}) = \lambda\chi_{E^2\lambda}(\boldsymbol{r}) \tag{A5}$$

holds for $\lambda = \pm 1$. By multiplying H to Eq. (A5) from the left side and by using Eq. (A1), we obtain the equation

$$\Gamma H\chi_{E^2\lambda}(\boldsymbol{r}) = -\lambda H\chi_{E^2\lambda}(\boldsymbol{r}). \tag{A6}$$

We find that $H\chi_{E^2\lambda}(\boldsymbol{r})$ is the eigenstate of Γ belonging to $-\lambda$. Thus we can connect $\chi_{E^2+}(\boldsymbol{r})$ and $\chi_{E^2-}(\boldsymbol{r})$ as

$$H\chi_{E^2\lambda}(\boldsymbol{r}) = c_{E^2\lambda}\chi_{E^2-\lambda}(\boldsymbol{r}), \tag{A7}$$

where $c_{E^2\lambda}$ is a constant.

A one-to-one correspondence exists between $\varphi_E(\boldsymbol{r})$ and $\chi_{E^2}(\boldsymbol{r})$. At first, we consider zero-energy states $\chi_{0\lambda}(\boldsymbol{r})$ which satisfy

$$H^2\chi_{0\lambda}(\boldsymbol{r}) = 0, \tag{A8}$$

in Eq. (A4). The integration of $\boldsymbol{r}$ after multiplying $\chi^\dagger_{0\lambda}(\boldsymbol{r})$ from the left results in

$$\int d\boldsymbol{r}\,|H\chi_{0\lambda}(\boldsymbol{r})|^2 = 0. \tag{A9}$$

This means that the norm of $H\chi_{0\lambda}(\boldsymbol{r})$ is zero. Therefore we conclude that

$$H\chi_{0\lambda}(\boldsymbol{r}) = 0. \tag{A10}$$

As a result, we find the relation

$$\varphi_{0\lambda}(\boldsymbol{r}) = \chi_{0\lambda}(\boldsymbol{r}). \tag{A11}$$

When a zero-energy state is described by $\varphi_{0+}(\boldsymbol{r}) = \chi_{0+}(\boldsymbol{r})$, the relations in Eqs. (A7) and (A10) suggest that $\chi_{0-}(\boldsymbol{r}) = 0$. Therefore the zero-energy states are always the eigenstates of Γ.

For $E \neq 0$, it is possible to represent $\varphi_E(\boldsymbol{r})$ by $\chi_{E^2\pm}(\boldsymbol{r})$. By calculating the norm of $H\chi_{E^2\lambda}(\boldsymbol{r})$, we obtain

$$E^2 = |c_{E^2\lambda}|^2. \tag{A12}$$

Multiplying H to Eq. (A7) from the left alternatively gives a relation

$$c_{E^2\lambda}c_{E^2-\lambda} = 1. \tag{A13}$$

Therefore, we find the relation

$$H\chi_{E^2\lambda}(\boldsymbol{r}) = Ee^{i\lambda\theta_{E^2}}\chi_{E^2-\lambda}(\boldsymbol{r}). \tag{A14}$$

Although we cannot fix the phase factor θ_{E^2}, it is possible to express the states $\varphi_E(\boldsymbol{r})$ for $E \neq 0$ as

$$\varphi_E(\boldsymbol{r}) = \frac{1}{\sqrt{2}}\left[e^{-i\theta_{E^2}/2}\chi_{E^2+}(\boldsymbol{r}) + s_E e^{i\theta_{E^2}/2}\chi_{E^2-}(\boldsymbol{r})\right], \tag{A15}$$

$$s_E = \begin{cases} 1 & \text{for } E > 0, \\ -1 & \text{for } E < 0. \end{cases} \tag{A16}$$

The nonzero-energy states are constructed by a pair of eigenstates of Γ: one belongs to $\lambda = 1$ and the other belongs $\lambda = -1$. Therefore, the states with $E \neq 0$ are not the eigenstates of Γ.

APPENDIX B: UNITARY TRANSFORMATION

The BdG Hamiltonian of the Dresselhaus nanowire represented by

$$\check{H}_0 = \begin{bmatrix} \hat{h} & i\Delta_0\hat{\sigma}_2 \\ -i\Delta_0\hat{\sigma}_2 & -\hat{h}^* \end{bmatrix}, \tag{B1}$$

$$\hat{h} = \xi_{\boldsymbol{r}}\hat{\sigma}_0 - V_{ex}\hat{\sigma}_1 + i\lambda_D\partial_x\hat{\sigma}_3, \tag{B2}$$

is transformed as follows. By using the unitary matrix

$$\check{R} = \begin{bmatrix} \hat{r} & 0 \\ 0 & \hat{r}^* \end{bmatrix}, \quad \hat{r} = \frac{1}{\sqrt{2}}\begin{bmatrix} e^{-i\pi/4} & -e^{-i\pi/4} \\ e^{i\pi/4} & e^{i\pi/4} \end{bmatrix}, \tag{B3}$$

the BdG Hamiltonian $\check{H}_0$ is first transformed to

$$\check{H}' = \check{R}\check{H}_0\check{R}^\dagger = \begin{bmatrix} \hat{h}' & i\Delta_0\hat{\sigma}_2 \\ -i\Delta_0\hat{\sigma}_2 & -\hat{h}' \end{bmatrix}, \tag{B4}$$

$$\hat{h}' = \xi_{\boldsymbol{r}}\hat{\sigma}_0 + V_{ex}\hat{\sigma}_3 + i\lambda_D\partial_x\hat{\sigma}_2. \tag{B5}$$

The Hamiltonian in this basis is represented only by real numbers. Next we apply a transformation which is similar to the Foldy-Wouthysen transformation [36] to the BdG Hamiltonian in Eq. (B4). Using a unitary matrix

$$\check{U} = \begin{bmatrix} \hat{u} & 0 \\ 0 & \hat{u} \end{bmatrix}, \tag{B6}$$

$$\hat{u} = \exp[i\hat{S}],\ \hat{S} = \frac{\lambda_D}{2\hbar V_{ex}}p_x\hat{\sigma}_1, \tag{B7}$$

with $p_x = -i\hbar\partial_x$, we transform H' into

$$\check{U}\check{H}'\check{U}^\dagger = \begin{bmatrix} e^{i\hat{S}}\hat{h}'e^{-i\hat{S}} & e^{i\hat{S}}(i\Delta_0\hat{\sigma}_2)e^{-i\hat{S}} \\ -e^{i\hat{S}}(i\Delta_0\hat{\sigma}_2)e^{-i\hat{S}} & -e^{i\hat{S}}\hat{h}'e^{-i\hat{S}} \end{bmatrix}. \tag{B8}$$

The diagonal term of Eq. (B4) can be expanded as

$$e^{i\hat{S}}\hat{h}'e^{i\hat{S}} = \hat{h}' + i[\hat{S},\hat{h}'] + \frac{i^2}{2!}[\hat{S},[\hat{S},\hat{h}']] + \cdots, \tag{B9}$$

with using the Baker-Housdorff formula. We assume large enough Zeeman potential so that $\alpha_D = \lambda_D k_F/V_{ex} \ll 1$ is satisfied where $k_F = \sqrt{2m\mu}/\hbar$ denotes Fermi wave number. From this assumption, we obtain

$$e^{i\hat{S}}\hat{h}e^{i\hat{S}} = \xi\hat{\sigma}_0 + V_{ex}\hat{\sigma}_3 + O(\alpha_D^2), \tag{B10}$$

within the first order of α_D. The off-diagonal term corresponding to the pair potential is transformed to

$$\begin{aligned} e^{i\hat{S}}(i\Delta_0\hat{\sigma}_2)e^{-i\hat{S}} &= i\Delta_0\hat{\sigma}_2 + i[\hat{S},i\Delta_0\hat{\sigma}_2] + \cdots \\ &= i\Delta_0\hat{\sigma}_2 - i\frac{\lambda_D\Delta_0}{\hbar V_{ex}}p_x\hat{\sigma}_3 + O(\alpha_D^2), \end{aligned} \tag{B11}$$

where we assume the uniform pair potential (i.e., $[p_x,\Delta_0] = 0$). As a result, the BdG Hamiltonian can be written as

$$\check{U}\check{H}'\check{U}^\dagger = \begin{bmatrix} \xi_{\boldsymbol{r}} + V_{ex} & 0 & -i\frac{\lambda_D\Delta_0}{\hbar V_{ex}}p_x & \Delta_0 \\ 0 & \xi_{\boldsymbol{r}} - V_{ex} & -\Delta_0 & i\frac{\lambda_D\Delta_0}{\hbar V_{ex}}p_x \\ i\frac{\lambda_D\Delta_0}{\hbar V_{ex}}p_x & -\Delta_0 & -\xi_{\boldsymbol{r}} - V_{ex} & 0 \\ \Delta_0 & -i\frac{\lambda_D\Delta_0}{\hbar V_{ex}}p_x & 0 & -\xi_{\boldsymbol{r}} + V \end{bmatrix} + O(\alpha_D^2). \tag{B12}$$

By interchanging the second column and the third one, and by interchanging the second row and the third one, the Hamiltonian can be deformed as

$$\check{H}_1 = \check{H}_P + \check{V}_\Delta, \tag{B13}$$

$$\check{H}_P = \begin{bmatrix} \hat{H}_\uparrow & 0 \\ 0 & \hat{H}_\downarrow \end{bmatrix}, \tag{B14}$$

$$\hat{H}_\sigma = \begin{bmatrix} \xi_{\boldsymbol{r}} + s_s V_{ex} & -s_s i \frac{\lambda_D \Delta_0}{\hbar V_{ex}} p_x \\ s_s i \frac{\lambda_D \Delta_0}{\hbar V_{ex}} p_x & -\xi_{\boldsymbol{r}} - s_s V_{ex} \end{bmatrix}, \tag{B15}$$

$$\check{V}_\Delta = \begin{bmatrix} 0 & i\Delta_0 \hat{\sigma}_2 \\ -i\Delta_0 \hat{\sigma}_2 & 0 \end{bmatrix}, \tag{B16}$$

$$s_s = \begin{cases} 1 & \text{for } \sigma = \uparrow, \\ -1 & \text{for } \sigma = \downarrow. \end{cases} \tag{B17}$$

These are the starting Hamiltonian in the analytic calculation.

We find that $\check{H}_1$ preserves chiral symmetry

$$\Gamma \check{H}_1 \Gamma^{-1} = -\check{H}_1, \quad \Gamma = \begin{bmatrix} \hat{\sigma}_1 & 0 \\ 0 & \hat{\sigma}_1 \end{bmatrix}. \tag{B18}$$

Finally, we discuss the symmetry property of H_0 in Eq. (B1) in its original basis. It is easy to show that $\check{H}_0$ satisfies the relations

$$\check{\Gamma}_0 \check{H}_0 \check{\Gamma}_0^{-1} = -\check{H}_0, \quad \check{\Gamma}_0 = \begin{bmatrix} 0 & -i\hat{\sigma}_1 \\ i\hat{\sigma}_1 & 0 \end{bmatrix}, \tag{B19}$$

which represents the chiral symmetry. The Hamiltonian $\check{H}_0$ also satisfies

$$\check{\Xi}_0 \check{H}_0 \check{\Xi}_0^{-1} = -\check{H}_0, \quad \check{\Xi}_0 = \begin{bmatrix} 0 & \mathcal{K}\hat{\sigma}_0 \\ \mathcal{K}\hat{\sigma}_0 & 0 \end{bmatrix}, \tag{B20}$$

where $\check{\Xi}_0$ represents the charge conjugation with $\mathcal{K}$ meaning the complex conjugation. The first equation in Eq. (B20) represents the particle-hole symmetry.

[1] Y. Tanaka, Y. Asano, A. A. Golubov, and S. Kashiwaya, Phys. Rev. B **72**, 140503(R) (2005).
[2] Y. Tanaka and A. A. Golubov, Phys. Rev. Lett. **98**, 037003 (2007).
[3] Y. Asano, Y. Tanaka, and S. Kashiwaya, Phys. Rev. Lett. **96**, 097007 (2006).
[4] Y. Tanaka and S. Kashiwaya, Phys. Rev. B **70**, 012507 (2004).
[5] Y. Asano, Y. Tanaka, A. A. Golubov, and S. Kashiwaya, Phys. Rev. Lett. **99**, 067005 (2007).
[6] Y. Asano, A. A. Golubov, Ya. V. Fominov, and Y. Tanaka, Phys. Rev. Lett. **107**, 087001 (2011).
[7] E. Majorana, Nuovo Cimento **14**, 171 (1937).
[8] F. Wiczek, Nat. Phys. **5**, 614 (2009).
[9] A. P. Schnyder, S. Ryu, A. Furusaki, and A. W. W. Ludwig, Phys. Rev. B **78**, 195125 (2008).
[10] M. Sato, Y. Tanaka, K. Yada, and T. Yokoyama, Phys. Rev. B **83**, 224511 (2011).
[11] J. D. Sau, R. M. Lutchyn, S. Tewari, and S. Das Sarma, Phys. Rev. Lett. **104**, 040502 (2010).
[12] R. M. Lutchyn, J. D. Sau, and S. Das Sarma, Phys. Rev. Lett. **105**, 077001 (2010).
[13] Y. Oreg, G. Refael, and F. von Oppen, Phys. Rev. Lett. **105**, 177002 (2010).
[14] M. Sato and S. Fujimoto, Phys. Rev. B **79**, 094504 (2009).
[15] A. C. Potter and P. A. Lee, Phys. Rev. Lett. **105**, 227003 (2010); Phys. Rev. B **83**, 094525 (2011).
[16] R. M. Lutchyn, T. D. Stanescu, and S. Das Sarma, Phys. Rev. Lett. **106**, 127001 (2011).
[17] M. Gibertini, F. Taddei, M. Polini, and R. Fazio, Phys. Rev. B **85**, 144525 (2012).
[18] V. Mourik, K. Zuo, S. M. Frolov, S. R. Plissard, E. P. A. M. Bakkers, and L. P. Kouwenhoven, Science **336**, 1003 (2012).
[19] M. T. Deng, C. L. Yu, G. Y. Huang, M. Larsson, P. Caroff, and H. Q. Xu, Nano Lett. **12**, 6414 (2012).
[20] A. Das, Y. Ronen, Y. Most, Y. Oreg, M. Heiblum, and H. Shtrikman, Nat. Phys. **8**, 887 (2012).
[21] A. D. K. Finck, D. J. Van Harlingen, P. K. Mohseni, K. Jung, and X. Li, Phys. Rev. Lett. **110**, 126406 (2013).
[22] B. A. Bernevig, J. Orenstein, and S.-C. Zhang, Phys. Rev. Lett. **97**, 236601 (2006).
[23] M. Kohda, V. Lechner, Y. Kunihashi, T. Dollinger, P. Olbrich, C. Schonhuber, I. Caspers, V. V. Belkov, L. E. Golub, D. Weiss, K. Richter, J. Nitta, and S. D. Ganichev, Phys. Rev. B **86**, 081306(R) (2012).
[24] G. Dresselhaus, Phys. Rev. **100**, 580 (1955).
[25] J. Alicea, Phys. Rev. B **81**, 125318 (2010).
[26] J. You, C. H. Oh, and V. Vedral, Phys. Rev. B **87**, 054501 (2013).
[27] S. Tewari and J. D. Sau, Phys. Rev. Lett. **109**, 150408 (2012).
[28] Y. Niu, S. B. Chung, C.-H. Hsu, I. Mandal, S. Raghu, and S. Chakravarty, Phys. Rev. B. **85**, 035110 (2012).
[29] M. Diez, J. P. Dahlhaus, M. Wimmer, and C. W. J. Beenakker, Phys. Rev. B **86**, 094501 (2012).
[30] G. E. Blonder, M. Tinkham, and T. M. Klapwijk, Phys. Rev. B **25**, 4515 (1982).
[31] P. A. Lee and D. S. Fisher, Phys. Rev. Lett. **47**, 882 (1981).
[32] T. Ando, Phys. Rev. B **44**, 8017 (1991).
[33] D. S. Fisher and P. A. Lee, Phys. Rev. B **23**, 6851 (1981).
[34] Y. Asano and Y. Tanaka, Phys. Rev B **87**, 104513 (2013).
[35] Y. Tanaka and S. Kashiwaya, Phys. Rev. Lett. **74**, 3451 (1995).
[36] L. L. Foldy and S. S. Wouthuysen, Phys. Rev. **78**, 29 (1950).